5 | Constraining the AGN formation channel for detected black hole binary mergers up to z=1.5 with the Quaia catalogue

Abstract

Statistical analyses based on the spatial correlation between the sky maps of Gravitational Wave (GW) events and the positions of potential host environments are a powerful tool to infer the origin of the black hole binary mergers that have been detected by the LIGO, Virgo, and KAGRA instruments. In this paper, we tighten our previous constraints on the fraction of detected GW events that may have originated from Active Galactic Nuclei (AGN). We consider 159 mergers detected not later than June 1st, 2024, and the all-sky quasar catalogue Quaia. We increase by a factor of 5.3 and 114 the number of considered GW sources and AGN respectively, also extending our analysis from redshift 0.3 to 1.5. This is possible thanks to the uniformity of the AGN catalogue and its high level of completeness, which we estimate as a function of redshift and luminosity. We find at a 95 per cent credibility level that un-obscured AGN with a bolometric luminosity higher than $10^{44.5}$erg s^{-1} (10^{45}erg s^{-1}) do not contribute to more than the 21 (11) per cent of the detected GW events.

5.1   Introduction

With the only exception of the Gravitational Wave (GW) event GW170817 (Abbott et al. 2017), a confident one-to-one association between the mergers of compact objects detected by the LIGO-Virgo-KAGRA (LVK) collaboration (Acernese et al. 2015; LIGO Scientific Collaboration et al. 2015; Akutsu et al. 2021) and their host galaxy is currently out of reach.

This is primarily caused by the typical size of the uncertainties that are associated to the sky position and to the luminosity distance of each GW event. The difficulty of associating each merger to its host environment hampers our ability to pin down the physical origin of the binary systems of which the coalescences have been directly measured. In one class of the possible formation scenarios that have been proposed (see Mapelli 2021, for a review) binaries of compact objects like binary black holes, binary neutron stars, and neutron star-black hole binaries are efficiently assembled and driven to merger in dense environments like globular clusters (Rodriguez et al. 2016) or nuclear stellar clusters (Chattopadhyay et al. 2023). In such hosts, binaries can have their semi-major axes shrunk by interactions with single objects. This binary hardening from single-binary encounters is important for the formation of systems that are able to merge within a Hubble time due to loss of orbital energy, emitted in the form of GWs. The least massive object of the three is expected to be ejected from the location of the single-binary interaction (Hills & Fullerton 1980; Ziosi et al. 2014), meaning that the hardened remnant binary will be composed by the two heaviest elements that partake in the encounter.

Another reason why dynamically dense environments might be the hosts of the most massive mergers detected by the LVK collaboration is the fact that their escape velocities can be large enough to retain the recoil-kicked remnant of a coalescence, turning it into a potential component of a subsequent GW event. This "hierarchical merger" scenario might be a physical interpretation for the existence of stellar-mass Black Holes (sBHs) in the pair-instability mass gap (Gerosa & Berti 2017, 2019; Yang et al. 2019; Barrera & Bartos 2022). This discontinuity is predicted between $\approx 50 \mathrm{M}_\odot$ and $\approx 120 \mathrm{M}_\odot$ in the sBH mass spectrum as a consequence of the complete disruption of the core during the supernova event at the end of the life cycle of stars with very high masses, that are therefore expected to leave no remnant (Heger & Woosley 2002; Belczynski et al. 2016). However, the astrophysical mass distribution of sBHs predicted by the LVK collaboration shows evidence for the presence of objects in the pair-instability mass gap (Abbott et al. 2023a). This challenges the hypothesis that

all the merging systems detected by the LVK collaboration have originated from an isolated stellar binary.

Accretion discs of AGN are a unique type of potential host environment for the assembly and the merger of binaries of compact objects. The reason is that in this so-called "AGN formation channel" the binaries and their components are not expected to interact only with other stellar objects, but also with the gas the accretion disc consists of. Thanks to this interaction, the disc might for example capture compact objects that have orbits moderately inclined with respect to its plane (Ostriker 1983; Fabj et al. 2020; Nasim et al. 2023). These disc captures have the effect of increasing the number density of compact objects in the disc, where the binary formation can be gas-assisted (Tagawa et al. 2020; DeLaurentiis et al. 2023b; Rowan et al. 2023). Another process which, as far as the formation of merging binaries of compact objects is concerned, is typical of the AGN scenario is migration: the radial motion of compact objects orbiting around the central supermassive black hole. Inward migration takes place in AGN discs where the net torque exerted by the gas onto the orbiting compact object is negative (Paardekooper et al. 2010; Bellovary et al. 2016), and can increase the number density of sBHs and neutron stars in the inner part of the accretion disc, facilitating the formation of binaries.

One possible way to put constraints on the fractional contribution of the AGN channel to the total merger rate of compact object binaries is through the investigation of the spatial correlation between the sky maps of the events detected by the LVK collaboration and the positions of observed AGN. This approach has been first suggested in Bartos et al. (2017a), where it was estimated that 300 GW detections are needed to statistically prove, with a significance of 3σ, the GW-AGN connection if half of the mergers happened in an AGN. In Corley et al. (2019) it was later found that the number of required detections decreases by a factor ≈ 3 if it is assumed that the inclination of the binary angular momentum with respect to the line of sight is known with an uncertainty of $5°$. In the simulated GW detections used in Bartos et al. (2017a) and Corley et al. (2019) the interferometers of LIGO and Virgo have been assumed to be working at design sensitivity. This level of instrumental sensitivity is a factor $\gtrsim 2$ better with respect to the one reached by the interferometers during the first three observing runs (Cahillane & Mansell 2022).

In Veronesi et al. (2022) the analysis presented in Bartos et al. (2017a) was repeated assuming a realistic distribution of the sizes of the 90 per cent Credibility Level (CL) localisation volumes (V90) of the mock GW detections. This distribution has been created by using the sensitivity curves that characterised the LIGO and Virgo interferometers during their third observing run (O3). It

was found that the amount of data collected during O3 would be enough to prove with a 3σ significance that the AGN channel contributes to half of the total merger rate only if the GW events originate form a rare host population with a number density lower than $10^{-7}\mathrm{Mpc}^{-3}$. Integrating the the AGN luminosity function of Hopkins et al. (2007), we find that this density corresponds to objects in the local Universe with a bolometric luminosity greater than approximately $10^{46}\mathrm{erg\ s}^{-1}$.

By building on this previous works, the first observational constraint on the efficiency of the AGN channel was put using the spatial-correlation approach in Veronesi et al. (2023), where the completeness of the quasar catalogues used during the cross-match with GW sky maps and the exact position of the potential host environments have been taken into account for the first time. By using catalogues of AGN with a spectroscopic estimate of redshift of $z \leq 0.3$ obtained from Milliquasv7.7b (Flesch 2021) and the sky maps of the 30 GW events detected in the same redshift range during the first three observing runs of the LVK collaboration, it was found that the fraction of the detected mergers that have originated in an AGN more luminous than $10^{45.5}\mathrm{erg\ s}^{-1}$ ($10^{46}\mathrm{erg\ s}^{-1}$) is not expected to be higher than 0.49 (0.17) at a CL of 95 per cent. A similar statistical investigation has been conducted also in Veronesi et al. (2024). In this case the sky maps of the GW events detected during O3 have been cross-matched spatially and temporally with the 20 unusual AGN flaring activities detected by the Zwicky Transient Facility (Bellm et al. 2019; Graham et al. 2019) that have been identified in Graham et al. (2023) as potential transient electromagnetic counterparts. We find no evidence for a correlation the GW events and the unusual flares. A similar result has been found in Palmese et al. (2021) analysing the spatial correlation between the event GW190521 and an unusual flaring activity of the AGN J124942.3+344929.

In this work we present new observational constraints on the fractional contribution of the AGN channel to the total merger rate, f_{AGN}. We use a spatial-correlation-based method similar to the one presented in Veronesi et al. (2023), and apply it to a larger dataset. In particular we use the sky maps of the GW events detected by the interferometers of the LVK collaboration up to June 1st, 2024, therefore including data coming from the fourth observing run (O4). This brings the total number of used sky maps to 159, which is more than five times the amount of GW events used in Veronesi et al. (2023). These are cross-matched with the AGN of the all-sky catalogue Quaia (Storey-Fisher et al. 2024), which is derived from the catalogue of extra-galactic quasar candidates published by the Gaia mission (Gaia Collaboration et al. 2023). The remarkable uniformity and completeness up to $z = 1.5$ of Quaia make it a relevant tool for

all-sky spatial correlation analyses like the one presented in this work.

In Section 5.2 we present the main characteristics of our dataset, which includes the different GW detections and the Quaia catalogue. In Section 5.3 we then describe the likelihood function that we maximise in order to obtain our new constraints on f_{AGN}, which are presented in Section 5.4. Finally, in Section 5.5, we draw the main conclusions regarding the AGN channel that can be inferred from the results of our analysis, and discuss about future developments of statistical spatial-correlation-based approaches. We adopt the cosmological parameters of the Cosmic Microwave Background observations by Planck (Planck Collaboration et al. 2016): $H_0 = (67.8 \pm 0.9)$ km s^{-1}Mpc^{-1}, $\Omega_{\mathrm{m}} = 0.308 \pm 0.012$, and $n_{\mathrm{s}} = 0.968 \pm 0.006$.

5.2   Datasets

In this section, we first present the main characteristics of the GW events the sky maps of which are used in our analysis. We then describe the main properties of the Quaia catalogue and how we estimate its completeness as a function of redshift for different sub-samples of it, characterised by different thresholds of bolometric luminosity, L_{bol}.

5.2.1   GW events

In this work we use the 159 sky maps of mergers of compact object binaries detected by the interferometers of the LVK collaboration up to June 1st, 2024. In particular, all the GW events from the first three observing runs are included, with the only exclusion of GW200308_173609 and of GW200322_091133. These two events are not taken into consideration because they are poorly localised, and the corresponding value of V90 cannot be estimated from the currently available posterior samples. Moreover, we use all the events from the first half of O4 (O4a) as well as all the events from its second half (O4b) that have been detected not later than June 1st, 2024. For this currently ongoing observing run, we select the detections that have a probability of being of terrestrial origin smaller than 1 per cent.

The sky maps of the events detected during the first three observing runs are downloaded from the Gravitational Wave Open Science Center (Abbott et al. 2023a). We use the posterior samples obtained using the IMRPhe-nomXPHM waveform model (Pratten et al. 2021) for all these events but

GW190425_081805, GW191219_163120, GW200105_162426, and
GW200115_042309. For these four events we use the Mixed posterior samples.

The sky maps of the 71 events of O4 are downloaded from the Gravitational-Wave Candidate Event Database [1], operated by the LIGO Scientific Collaboration. For each event, we use the most recent version of its sky map, which is either obtained from the Bilby localisation algorithm (Ashton et al. 2019) or from the Bayestar one (Singer & Price 2016).

Figure 5.1 shows the luminosity distance of all the 159 GW events used in this work as a function of V90. The median value of the luminosity distance (2012.3 Mpc) and of V90 ($7.67 \cdot 10^8 \mathrm{Mpc}^3$) are indicated by a horizontal dashed line and by a vertical one, respectively.

5.2.2   Quaia AGN catalogue

In order to obtain tight constraints of f_{AGN} with methods based on spatial correlation like the one used in this work, is important to use an AGN catalogue that has the highest possible value of completeness. This property of a catalogue is in general a function of the redshifts, the sky positions, and the luminosities of the objects it contains.

In the analysis here presented, the Quaia AGN catalogue (Storey-Fisher et al. 2024) [2] is cross-matched with the sky maps of the GW events detailed in Section 5.2.1. This is done once the completeness of such a catalogue has been estimated. Quaia is an all-sky catalogue is based on sources identified as quasar candidates in the third data release of the Gaia mission (Gaia Collaboration et al. 2023). The final version of this catalogue is obtained by selecting the objects that have an infrared counterpart in the unWISE catalogue (Lang 2014; Meisner et al. 2019) and by performing cuts in colours and proper motion in order to decrease the amount of contaminants (see Section 3.1 of Storey-Fisher et al. 2024, for details). The result is a catalogue containing 1,295,502 quasar candidates with a magnitude in the Gaia G-band $\mathrm{mag_G} < 20.5$. The redshifts of all these objects are estimated using a k-Nearest Neighbors model trained on the AGN present in Quaia of which the spectra are in the 16th Data Release (DR16Q) of the the Sloan Digital Sky Survey (SDSS) (Lyke et al. 2020).

Figure 5.2 shows the mollweide projection of the sky distribution of the AGN contained in the Quaia catalogue. The colour of each pixel depends on the amount of objects in the correspondent position in the sky. The size of each

---

[1] https://gracedb.ligo.org/

[2] All the data concerning the Quaia catalogue, and its modeled selection function are publicly available at https://zenodo.org/records/8060755.
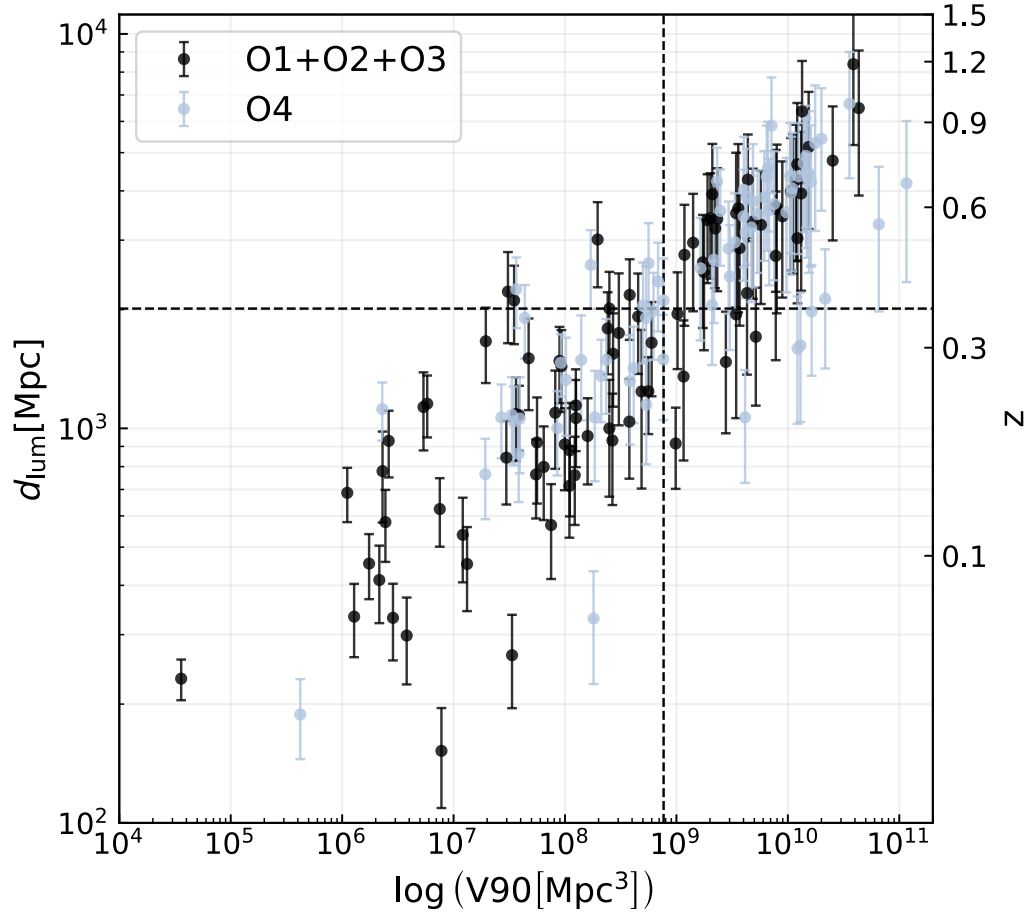
Figure 5.1: Luminosity distance as a function of V90 for the 159 GW events used in our analysis. The error bars represent an uncertainty of one standard deviation around the mean of the estimated distance. While the black markers indicate the mergers detected during the first three observing runs of the LVK collaboration, the light blue ones represent the events detected in O4, up to June 1st, 2024. The horizontal and the vertical dashed lines mark the median value of the luminosity distance estimates and of V90, respectively. In addition, we show the estimated redshift on the right axis.
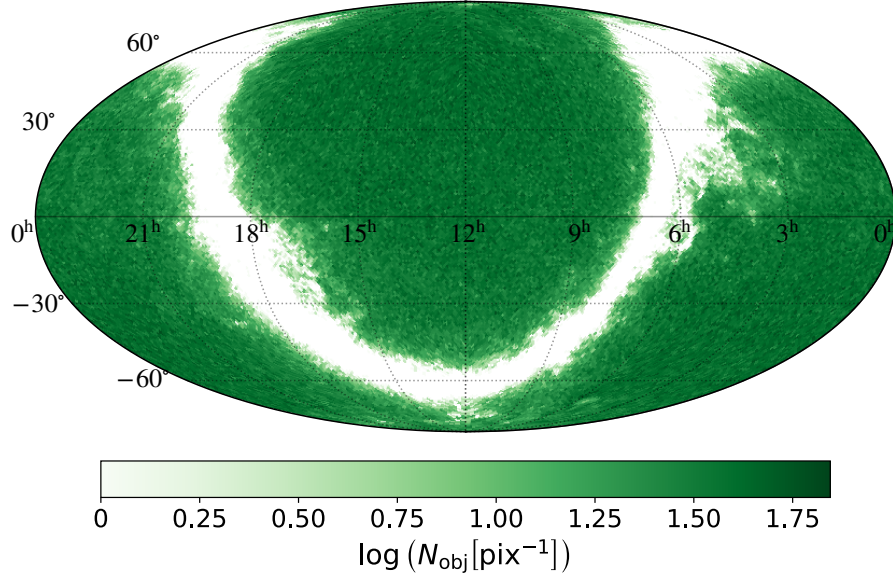
Figure 5.2: Mollweide projection of the sky positions in equatorial coordinates of the 1,295,502 objects contained in the Quaia catalogue with a magnitude $\text{mag}_{\text{G}} <$ 20.5. Different shades of green represent different sky-projected number densities. The resolution is the one of an HealPix map with NSIDE=64.

pixel is $\approx 2.557 \cdot 10^{-4}$ steradians. Its remarkable uniformity outside the region containing the Milky Way Galactic plane makes Quaia a useful tool for spatial correlation analyses between AGN and GW events.

The AGN here used during the cross-match with the GW sky maps are the 660,031 objects present in Quaia that have a redshift estimate not larger than $z = 1.5$ and that are in the region of the sky where the galactic latitude b is either higher than $10°$ or smaller than $-10°$. The redshift selection is performed since all the GW events used in this work are expected to have taken place in the $0 \leq z \leq 1.5$ range (see Figure 5.1). We choose not to use the objects with a small absolute value of galactic latitude for simplicity. We consider the density of objects in the catalogue to be independent from their Right Ascension or Declination, as long as they are outside of the region of the Galactic plane.

The selection function marginalised over redshift that has been modeled for Quaia highlights density variations in regions of the sky outside the Galactic plane (See Storey-Fisher et al. 2024, Figure 13). In this work thes selection effects are not taken into account, and we obtain estimates of the completeness of

Quaia using the sky-averaged number density of objects with the only exclusion of the Galactic plane (see Section 5.2.3). This choice is not expected to have a significant effect on our final results, because during the likelihood-maximisation process we use the average value of the catalogue's completeness inside the 90 per cent CL localisation volume for each GW event, and the sky projection of such regions is usually much greater than the typical angular size of the modeled number density variations.

The exclusion of the Galactic plane from Quaia removes only ≈ 1.6 per cent of all the objects within $z = 1.5$ and therefore is not expected to decrease notably the constraining power of our analysis.

5.2.3 Completeness estimation

The likelihood maximisation method presented in this work requires an estimate of the completeness of the AGN catalogue that is used. We therefore estimate this property of our Quaia AGN sample as a function of redshift and luminosity. We do so in three steps:

- Estimation of the bolometric luminosity of each object in Quaia with a redshift estimate not higher than $z = 1.5$. This sub-section of Quaia is later referred to as Quaia$_{z<1.5}$, and it differs from our sample used during the cross-match with GW sky maps only because in the latter the objects in the Galactic plane region have been removed. In Section 5.2.3.1 we describe how these luminosities are evaluated starting from the magnitudes in the Gaia G$_{\rm RP}$ band ($\rm mag_{G_{RP}}$);

- Comparison of the bolometric luminosities obtained from the Gaia measurements with the ones calculated from SDSS data and presented in Wu & Shen (2022). We do this for all the objects that are both in our sample of Quaia and in SDSS DR16Q, and then use the results of this comparison to correct the luminosity of each object in our catalogue. This step is done in order to have estimates of the luminosities that are compatible with the ones of SDSS, which is the survey used during the fit of the luminosity function we compare the number of objects in our catalogue with to calculate its completeness of our catalogue. The comparison between the luminosity estimates obtained from Gaia data and the ones from SDSS is detailed in Section 5.2.3.2.;

- Comparison between the number of objects present in our quasar sample in a specific redshift bin and the ones predicted by the AGN luminosity

function presented in Kulkarni et al. (2019). This is done five times, considering each time a different threshold in bolometric luminosity. The comparison with the quasar luminosity function and the final calculation of the completeness of our catalogue are delineated in Section 5.2.3.3.

5.2.3.1 Evaluation of bolometric luminosity from $\mathrm{mag}_{\mathrm{G_{RP}}}$:

To obtain an estimate of the bolometric luminosity of all the objects contained in $\mathrm{Quaia}_{z<1.5}$, we first calculate the flux density in photo-electrons per second using the following standard relation:

$$f_{\nu_{\mathrm{G_{RP}}}} \left[\frac{e^-}{s}\right] = 10^{-\frac{m_{\mathrm{G_{RP},VEG}} - \mathrm{ZP_{RP,VEG}}}{2.5}} \quad , \tag{5.1}$$

where $\mathrm{ZP_{RP,VEG}} = 24.7479$ is the photometric zero-point in the Vega system for the Gaia $\mathrm{G_{RP}}$ band. The flux density in Jansky is then calculated by multiplying $f_\nu \left[\frac{e^-}{s}\right]$ by the conversion factor $c_\nu = 3.299 \cdot 10^{-36} \mathrm{Jy} \cdot \mathrm{s}/e^-$. The values of $\mathrm{ZP_{RP,VEG}}$ and of c_ν are taken from the online documentation regarding the calibration of Gaia data [3].

The intrinsic luminosity of each AGN emitted at a rest-frame frequency of $\nu_{\mathrm{G_{RP}}} = 10^{14.588}\mathrm{Hz}$ [4] is then calculated as follows:

$$\nu_{\mathrm{G_{RP}}} L_{\nu_{\mathrm{G_{RP}}}} = \nu_{\mathrm{G_{RP}}} f_{\nu_{\mathrm{G_{RP}}}} \left(4\pi d_{\mathrm{lum}}^2\right) (1+z)^{-0.657} \quad , \tag{5.2}$$

where d_{lum} is the luminosity distance correspondent to the redshift z of each object. The last term of Equation 5.2 is used to take into account the shape of the typical Spectral Energy Distribution (SED) of the objects in Quaia. The value of the exponent is calculated from a linear fit of the mean SED of all SDSS quasars presented in Richards et al. (2006). In particular, in the range between $\nu_{\mathrm{G_{RP}}}$ and $(1 + z_{\mathrm{max}}) \nu_{\mathrm{G_{RP}}}$ (where, for $\mathrm{Quaia}_{z<1.5}$, $z_{\mathrm{max}} = 1.5$), we find that:

$$\log\left(\nu L_\nu\right) \propto \log\left(\nu\right) \cdot 0.657 \quad , \tag{5.3}$$

and therefore

$$\nu_{\mathrm{em}} L_{\nu_{\mathrm{em}}} = \nu_{\mathrm{G_{RP}}} L_{\nu_{\mathrm{G_{RP}}}} (1+z)^{0.657} \quad , \tag{5.4}$$

where $\nu_{\mathrm{em}} L_{\nu_{\mathrm{em}}}$ is the luminosity emitted in the rest-frame frequency that is observed at $\nu_{\mathrm{G_{RP}}}$.

The bolometric luminosity is then calculated by multiplying $\nu_{\mathrm{G_{RP}}} L_{\nu_{\mathrm{G_{RP}}}}$ by the value that the frequency-dependent bolometric correction presented in Richards et al. (2006) has at the frequency $\nu_{\mathrm{G_{RP}}}$. This value is 11.004.

---

[3] https://www.cosmos.esa.int/web/gaia-users/archive
[4] this value has been calculated assuming a fiducial wavelength for the $\mathrm{G_{RP}}$ band of 7750Å.

5.2.3.2   Comparison with the bolometric luminosity estimates of Wu & Shen (2022)

After computing the bolometric luminosities from the Gaia RP magnitudes following the procedure described in Section 5.2.3.1, we can now compare to the ones listed in the catalogue presented in Wu & Shen (2022). This catalogue contains continuum and emission-line properties of the 750,414 broad-line Quasars of SDSS DR16Q. Among these properties there is the bolometric luminosity of each AGN, estimated from the continuum luminosity at the rest-frame wavelengths of 5100, 3000, and 1350 Å. We perform a cross-match between this catalogue and $Quaia_{z<1.5}$, adopting to arcsec as matching radius. A total of 136,368 matches are found. For each of these AGN it is possible to calculate the difference between the logarithm of the bolometric luminosity estimated from $mag_{G_{RP}}$ and the logarithm of the bolometric luminosity taken from the catalogue of Wu & Shen (2022). The mean value of the distribution of this differences is 0.073, and its standard deviation is 0.213. The bolometric luminosities obtained from $mag_{G_{RP}}$ are on average slightly over-estimated. We then proceed to correct this difference.

We divide the AGN that are both in $Quaia_{z<1.5}$ and in the catalogue presented in Wu & Shen (2022) into five bolometric luminosity bins. This partition is performed using the estimates calculated starting from $mag_{G_{RP}}$. Each of these sub-samples is then divided in redshift bins, using the Quaia estimates of redshift. For each sub-sample in luminosity we choose a different number of linear redshift bins and a different value of the maximum redshift to consider, to ensure that in each of these bins there are at least 10 objects. In Table 5.1 we list the minimum and the maximum bolometric luminosity for each of the five sub-samples, the number of redshift bins in which it is divided, and the maximum redshift considered in this division.

For each bin in luminosity and redshift, we perform a linear fit between the logarithm of the bolometric luminosities estimated starting from $mag_{G_{RP}}$, and the one of the bolometric luminosities taken from the catalogue of Wu & Shen (2022). We therefore obtain one set of best-fit parameters for each bin in luminosity and redshift. We finally use these best-fit parameters to correct the bolometric luminosity estimated from $mag_{G_{RP}}$ of each object contained in our quasar sample. These adjusted estimates are the ones used in the rest of the analysis presented in this paper. The distribution of the difference between the logarithm of the original bolometric luminosities obtained from the Gaia magnitudes and the logarithm of their corrected version has a mean of 0.073 and a standard deviation of 0.027.

Table 5.1: Partition of the AGN contained both in Quaia$_{z<1.5}$ and in the catalogue presented in Wu & Shen (2022). This partition has been used to compare the estimates of bolometric luminosity. We list the minimum and the maximum luminosity of each sub-sample. To perform this subdivision we use the bolometric luminosity estimates that are obtained starting from mag$_{G_{RP}}$. In order to correct these estimates according to the values contained in the catalogue of Wu & Shen (2022), we divide each sub-sample of Quaia$_{z<1.5}$ in linear redshift bins. The number of these bins for each sub-sample and the maximum value of the redshift used in this division, which has been done using the Quaia redshift estimates, are listed in the last two columns.

$\log\left(L_{\mathrm{bol,min}}\left[\mathrm{erg\ s^{-1}}\right]\right)$	$\log\left(L_{\mathrm{bol,max}}\left[\mathrm{erg\ s^{-1}}\right]\right)$	$N_{\mathrm{bins,z}}$	z_{max}
46.5	-	4	1.5
46	46.5	5	1.5
45.5	46	8	1.5
45	45.5	9	1.1
-	45	3	0.5

5.2.3.3   Comparison with the AGN luminosity function of Kulkarni et al. (2019)

In order to have an estimate of the completeness of our Quaia sample as a function of redshift we compare the number of objects it contains with the expectation value calculated from the AGN luminosity function presented in Kulkarni et al. (2019). In particular we use the best-fit double power law function in which the parameters evolve as a function of redshift according to Model 1 (for the analytical expression see Equations 7, 13, 16, 17, and 18 of Kulkarni et al. 2019, while the best-fit parameters are listed in the first column of Table 3 of the same paper).

We compare the observed number of AGN with the predicted one for five different sub-samples of the catalogue. Each of these sub-samples is characterised uniquely by a different threshold in bolometric luminosity. We divide all the sub-samples into 8 linear redshift bins between $z = 0$ and $z = 1.5$. We calculate the expected number of objects in each bin by integrating the luminosity function of Kulkarni et al. (2019). We do this for each value of luminosity threshold. The luminosity function is expressed as a function of the absolute monochromatic AB magnitude at a rest frame of 1450Å. For this reason, in order to obtain the expected number of objects as a function of redshift for a specific threshold of bolometric luminosity, we first convert this luminosity in the UV rest frame magnitude. We do this using the magnitude-dependent

bolometric correction function presented in Runnoe et al. (2012).

The dashed lines in Figure 5.3 show linear interpolations of the number of expected AGN in all the different redshift bins, obtained through the integration of the luminosity function. Different colours correspond to different bolometric luminosity thresholds. The round markers correspond to the number of objects brighter than the same threshold luminosities that are contained in our quasar sample in the different redshift bins, divided by $1 - \sin(10°)$ to take into account our cut in galactic latitude. For comparison, the crosses show the number of objects in SDSS DR16Q for each redshift bin and luminosity threshold, divided by $A_{\mathrm{SDSS}}/A_{\mathrm{sky}}$, where $A_{\mathrm{SDSS}} = 9,376 \ \mathrm{deg}^2$ is the area of the footprint of SDSS, and $A_{\mathrm{sky}} = 41,253 \ \mathrm{deg}^2$ is the total area of the sky. We take the bolometric luminosities of the AGN in SDSS DR16Q from the catalogue presented in Wu & Shen (2022).

We can now compute the completeness for each redshift bin and for each different cut in bolometric luminosity dividing the sky-area-corrected number of observed AGN by the expected one. Whenever the former is greater than the latter, the completeness is set to one. Because of the selection in galactic latitude we perform, the completeness in the region where $|b| < 10°$ is zero. The values of the estimated completeness for all the different redshift bins and the different bolometric luminosity thresholds are listed in Table 5.2.

5.3   Method

Once the bolometric luminosity has been calculated for each AGN of our catalogue and the completeness of the latter has been estimated as a function of redshift and luminosity, we calculate the posterior probability distribution on f_{AGN}. To do so, we use a likelihood function similar to the ones used in Veronesi et al. (2023) and in Veronesi et al. (2024). The general analytical expression of this function is the following:

$$\mathcal{L}(f_{\mathrm{AGN}}) = \prod_{i=1}^{N_{\mathrm{GW}}} \mathcal{L}_i(f_{\mathrm{AGN}})$$
$$= \prod_{i=1}^{N_{\mathrm{GW}}} [c_i \cdot 0.90 \cdot f_{\mathrm{AGN}} \cdot \mathcal{S}_i + (1 - c_i \cdot 0.90 \cdot f_{\mathrm{AGN}}) \mathcal{B}_i] \quad , \qquad (5.5)$$

where $N_{\mathrm{GW}} = 159$ is the total number of mergers of binaries of compact objects we consider in the analysis, and c_i is the average completeness of the catalogue
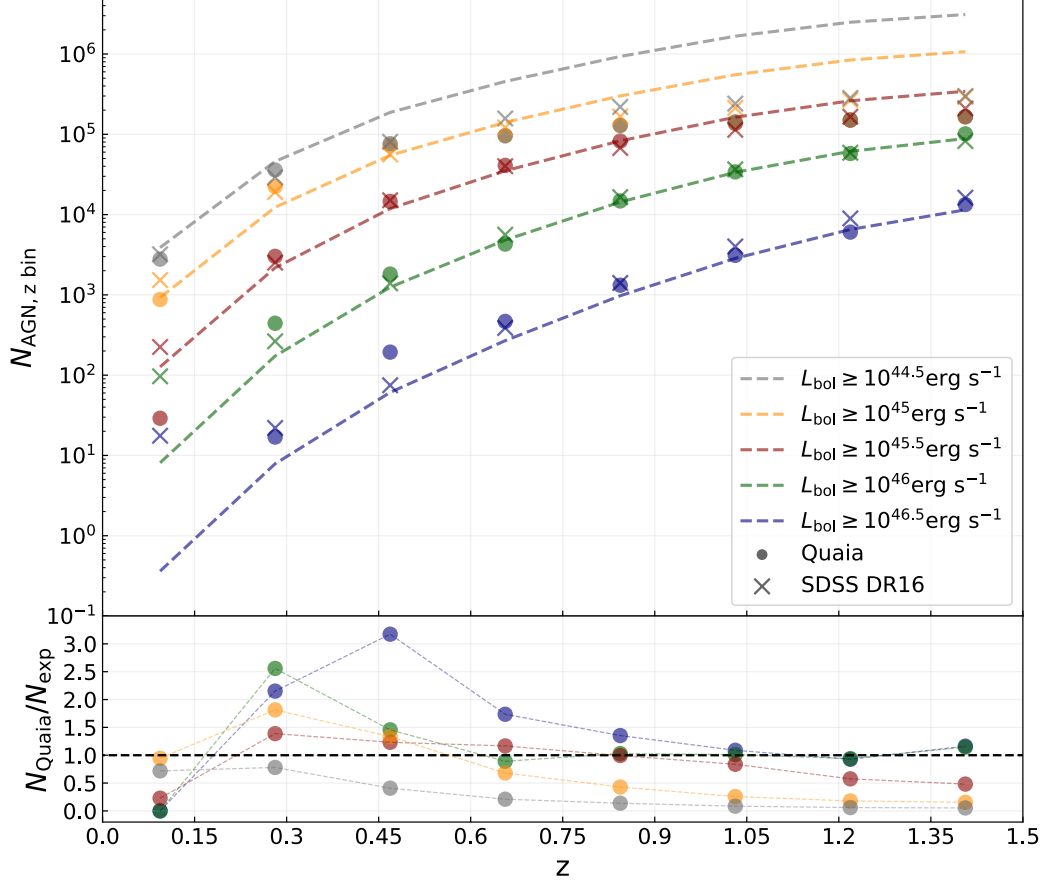
Figure 5.3: *Top panel:* Comparison between the expected number of AGN in specific redshift bins as a function of different bolometric luminosity thresholds (dashed lines) and the observed number of objects contained in our Quaia sample (round markers) and in SDSS DR16 (cross markers). The expected numbers have been calculated integrating the redshift-evolving luminosity function presented in Kulkarni et al. (2019). Only the objects that have an absolute value of galactic latitude greater than 10° are in our catalogue, and the area of the SDSS footprint is ≈ 22.7 per cent of the entire sky area. The numbers of observed AGN have been renormalized according to this. *Bottom panel:* Ratio between the number of AGN in Quaia (N_{Quaia}) and the expected one (N_{exp}), as a function of redshift. Different colors represent the same different luminosity thresholds of the top panel. The measured decrease of the completeness as a function of redshift above $z \approx 0.3$, and the fact that this value goes significantly below unity for the sub-samples with the three lowest luminosity thresholds, are due to the flux limit of Gaia. We consider the completeness of our catalogue to be 100 per cent in each bin where $N_{\mathrm{Quaia}} \geq N_{\mathrm{exp}}$.

Table 5.2: Estimated completeness of our Quaia sample in the region of the sky with a galactic latitude greater than $10°$ or smaller than $-10°$. All the values are between 0 and 1, rounded up to the third decimal digit, and are listed for 8 linear redshift bins as a function of 5 different bolometric luminosity thresholds.

	$\log\left(L_{\mathrm{bol}}\,[\mathrm{erg\,s^{-1}}]\right) \geq 46.5$	$\log\left(L_{\mathrm{bol}}\,[\mathrm{erg\,s^{-1}}]\right) \geq 46.0$	$\log\left(L_{\mathrm{bol}}\,[\mathrm{erg\,s^{-1}}]\right) \geq 45.5$	$\log\left(L_{\mathrm{bol}}\,[\mathrm{erg\,s^{-1}}]\right) \geq 45$	$\log\left(L_{\mathrm{bol}}\,[\mathrm{erg\,s^{-1}}]\right) \geq 44.5$
$0.0000 < z \leq 0.1875$	0	0	0.229	0.945	0.718
$0.1875 < z \leq 0.3750$	1	1	1	1	0.781
$0.3750 < z \leq 0.5625$	1	1	1	1	0.408
$0.5625 < z \leq 0.7500$	1	0.891	0.994	0.681	0.211
$0.7500 < z \leq 0.9375$	1	1	0.837	0.429	0.138
$0.9375 < z \leq 1.1250$			0.576	0.258	0.085
$1.1250 < z \leq 1.3125$	0.927	0.940	0.482	0.179	0.060
$1.3125 < z \leq 1.5000$	1	1		0.155	0.053

in the region occupied by the 90 per cent CL localisation volume of the i-th GW event. The 0.9 factor that multiplies f_{AGN} is used to take into account that we use 90 per cent CL localisation volumes, therefore only in the 90 per cent of the time the true sources are expected to be within them.

For every GW event we calculate one value of c_i for each different bolometric luminosity threshold we use in our analysis. Figure 5.4 shows the Cumulative Distribution Function (CDF) of c_i for all these different sub-samples. Different colours indicate different luminosity thresholds. The sub-samples with a thresh-
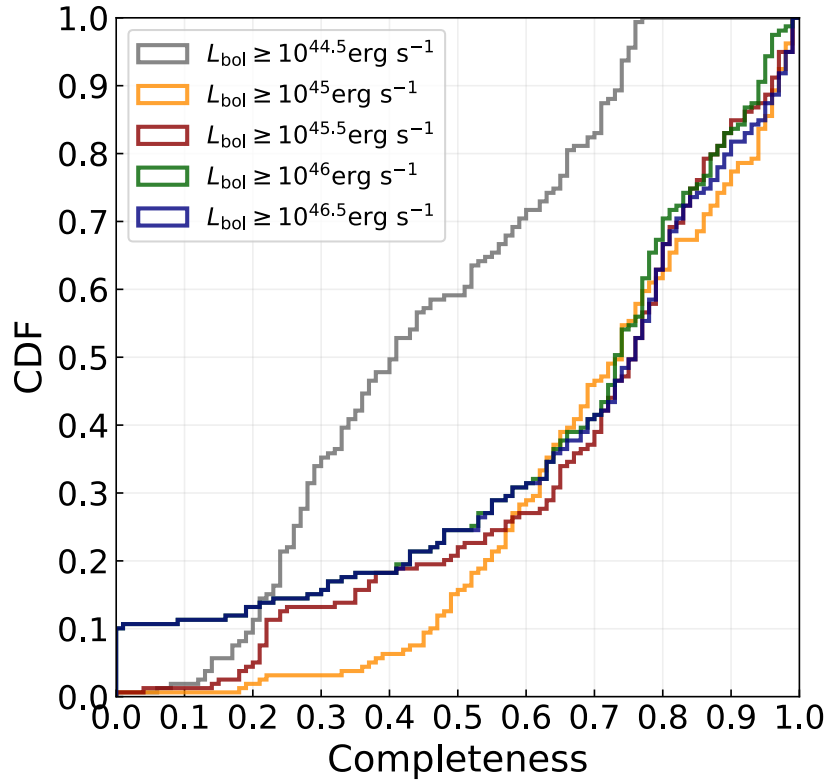
Figure 5.4: CDF of the values of the average completeness of our AGN catalogue in the region contained within the 90 per cent CL localisation volume of each of the 159 GW events used in this work. Different colours correspond to different sub-samples of the catalogue. Each of these sub-samples is uniquely characterised by a different value of bolometric luminosity threshold.

old luminosity of $10^{46}\mathrm{erg\ s^{-1}}$ and of $10^{46.5}\mathrm{erg\ s^{-1}}$, and that therefore contain

only the most luminous and rare AGN, have a null completeness at low redshift. For this reason ≈ 10 per cent of the GW events have $c_i = 0$ when those two catalogues are considered.

In Equation 5.5, $\mathcal{S}_i$ is the signal probability density and is calculated as follows:

$$\mathcal{S}_i = \frac{1}{V90_i} \sum_{j=1}^{N_{\mathrm{AGN,V90}_i}} \frac{p_j}{n_{\mathrm{AGN},j}} \quad , \tag{5.6}$$

where $N_{\mathrm{AGN,V90}_i}$ is the number of AGN located within the 90 per cent CL localisation volume of the i-th GW event, which has a size of $V90_i$, and p_j, measured in Mpc^{-3}, is the probability density representing how likely it is that the i-th merger has happened in the exact position of the j-th AGN. Finally, $n_{\mathrm{AGN},j}$ is the number density of the AGN catalogue in the redshift bin where the j-th AGN is. The value of this number density for each AGN has been obtained by dividing the total number of objects in the redshift bin in which it is located by the comoving volume enclosed in such a bin, excluding the region in which $|b| < 10°$.

The background probability density is calculated as follows:

$$\mathcal{B}_i = \frac{0.9}{V90_i} \quad , \tag{5.7}$$

where, in analogy to what has been done in Veronesi et al. (2023) and in Veronesi et al. (2024), the 0.9 factor ensures that $\mathcal{B}_i$ and $\mathcal{S}_i$ have the same normalisation.

We cross-match the sky maps of the 159 GW events with the 5 different subsamples of the AGN catalogue separately, using the `postprocess.crossmatch` function of the package `ligo.skymap`. The results of these cross-matches are used to evaluate $\mathcal{L}(f_{\mathrm{AGN}})$ using Equation 5.5. We then calculate the posterior probability distribution normalising the likelihood function and assuming a uniform prior on f_{AGN} in the $[0, 1]$ range.

5.4   Results

The posterior probability on f_{AGN} peaks at $f_{\mathrm{AGN}} = 0$ independently on which bolometric luminosity threshold we consider. In Figure 5.5 is shown in blue the region of the investigated parameter space that our analysis rejects with a credibility of 95 per cent.

We show the comparison with previous results, obtained in Veronesi et al. (2023) using a more limited dataset. This consisted of three catalogues, char-

acterised by three different cuts in bolometric luminosity, of spectroscopically identified AGN with redshift $z \leq 0.3$, that have been cross-matched with the 30 GW events detected in the same redshift range during the first three observing runs of the LVK collaboration. These quasar catalogues are selected from the version 7.7b of the Milliquas catalogue (Flesch 2021).

The increase of a factor ≈ 5 in the number of sky maps used in the analysis here presented and the high level of completeness of our Quaia sample in the redshift range we consider are the causes of the increase in the constraining power with respect to our previous work.

In Table 5.3 we list how many objects are considered during the cross-matches, what fraction of our catalogue they consist of, and the upper limits we put on f_{AGN} at 68, 90, and 95 per cent credibility.

The 95 per cent CL upper limit on the fraction of the detected GW events that originated in an un-obscured AGN brighter than $10^{44.5}$erg s^{-1} is 21 per cent. Considering rarer, brighter quasars, the constraints become tighter. In fact we find with the same level of credibility that no more than 11 per cent of the mergers come from an AGN brighter than 10^{45}erg s^{-1}. This increase of constraining power is primarily caused by the fact that the AGN catalogue with the higher luminosity threshold has a higher level of estimated completeness (See Figure 5.4). Further increasing the value of the luminosity threshold does not lead to significantly more stringent constraints.

Figure 5.6 shows the logarithm of the ratio between the single-event likelihoods ($\mathcal{L}_i$) calculated at $f_{\mathrm{AGN}} = 1$ and the ones calculated at $f_{\mathrm{AGN}} = 0$, as a function of V90$_i$. Different panels correspond to different bolometric luminosity thresholds. In each plot the markers are coloured according to the average completeness inside the localisation volume of the corresponding merger. The dashed horizontal lines indicate where the logarithm has a null value, therefore where $\mathcal{L}_i\left(f_{\mathrm{AGN}} = 1\right) = \mathcal{L}_i\left(f_{\mathrm{AGN}} = 0\right)$. The markers above these lines correspond to GW events for which the hypothesis of random-chance association between merger sky maps and AGN is disfavoured.

One candidate GW event in particular, S240511i, detected during the second half of O4, corresponds to a value of $\mathcal{L}_i\left(f_{\mathrm{AGN}} = 1\right)/\mathcal{L}_i\left(f_{\mathrm{AGN}} = 0\right)$ which is greater than one, independently from the luminosity threshold. The corresponding marker is particularly evident in top part of the first two panels of Figure 5.6. In the case of the cross-match with the sub-sample of our catalogue with AGN brighter than $10^{46.5}$erg s^{-1} (10^{46}erg s^{-1}), for this GW event $\log\left(\mathcal{L}_i\left(f_{\mathrm{AGN}} = 1\right)/\mathcal{L}_i\left(f_{\mathrm{AGN}} = 0\right)\right) \approx 1.32$ (0.72). In particular, two AGN brighter than $10^{46.5}$erg s^{-1} are found within the 90 per cent CL localisation volume, which in the case of this GW event has a size of V90 $\approx 10^{7.64}$Mpc^3.
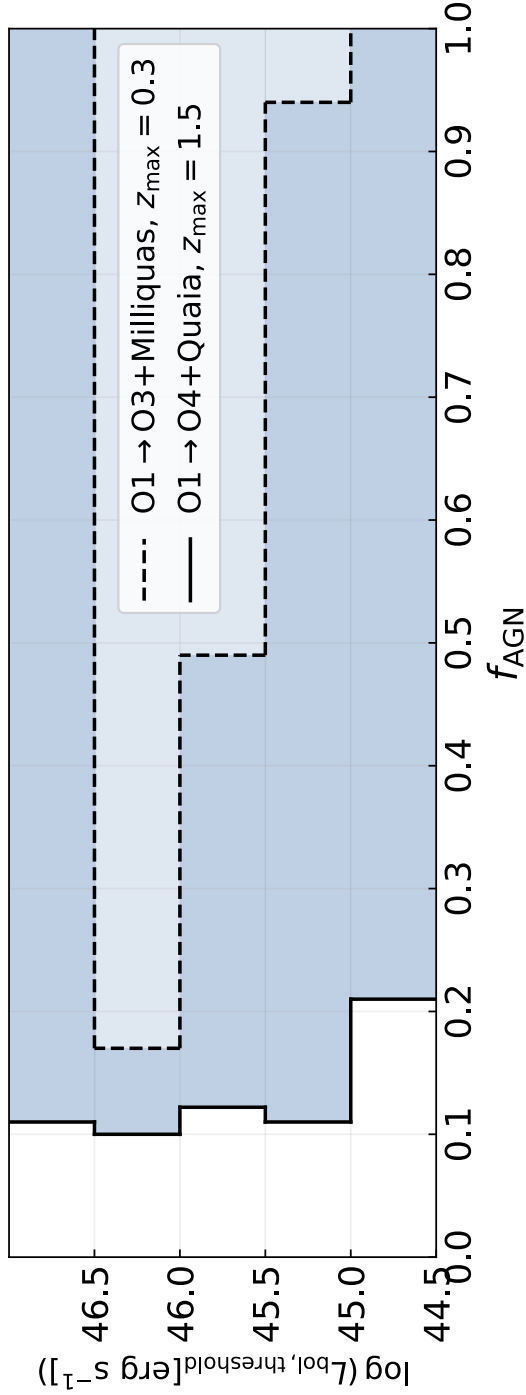
Figure 5.5: Observational constraints on f_{AGN} based on spatial correlation. The blue region of the plot shows the part of the parameter space we investigated that is rejected by our analysis at a 95 per cent CL. The region enclosed in in the dashed line shows the results obtained with a more limited dataset in Veronesi et al. (2023). Such previous work used the 30 GW events detected in the first three observing runs of the LVK collaboration that are located within $z = 0.3$ at a 90 per cent CL, and three different catalogues of AGN in the same redshift range. The region enclosed in the solid line shows the results of this work, which explores a wider range of AGN luminosities and uses all the mergers of binaries of compact objects directly detected up until June 1st, 2024.

Table 5.3: Upper limits on f_{AGN} we obtain at different levels of credibility, for the five cuts in bolometric luminosity we consider. For each of such cuts we also list the number of AGN used in the analysis ($N_{\mathrm{AGN,cut}}$), and what fraction of the total number of AGN in our catalogue ($N_{\mathrm{AGN,tot}}$) they consist of. All the values in this table have been rounded up to the second decimal digit.

$\log\left(L_{\mathrm{bol,threshold}}\;[\mathrm{erg\;s^{-1}}]\right)$	$N_{\mathrm{AGN,cut}}$	$N_{\mathrm{AGN,cut}}/N_{\mathrm{AGN,tot}}$	68 per cent upper limit	90 per cent upper limit	95 per cent upper limit
46.5	20,236	0.03	0.05	0.09	0.11
46	177,117	0.27	0.04	0.08	0.10
45.5	490,628	0.74	0.05	0.10	0.13
45	644,393	0.98	0.05	0.09	0.11
44.5	659,949	1.00	0.08	0.16	0.21
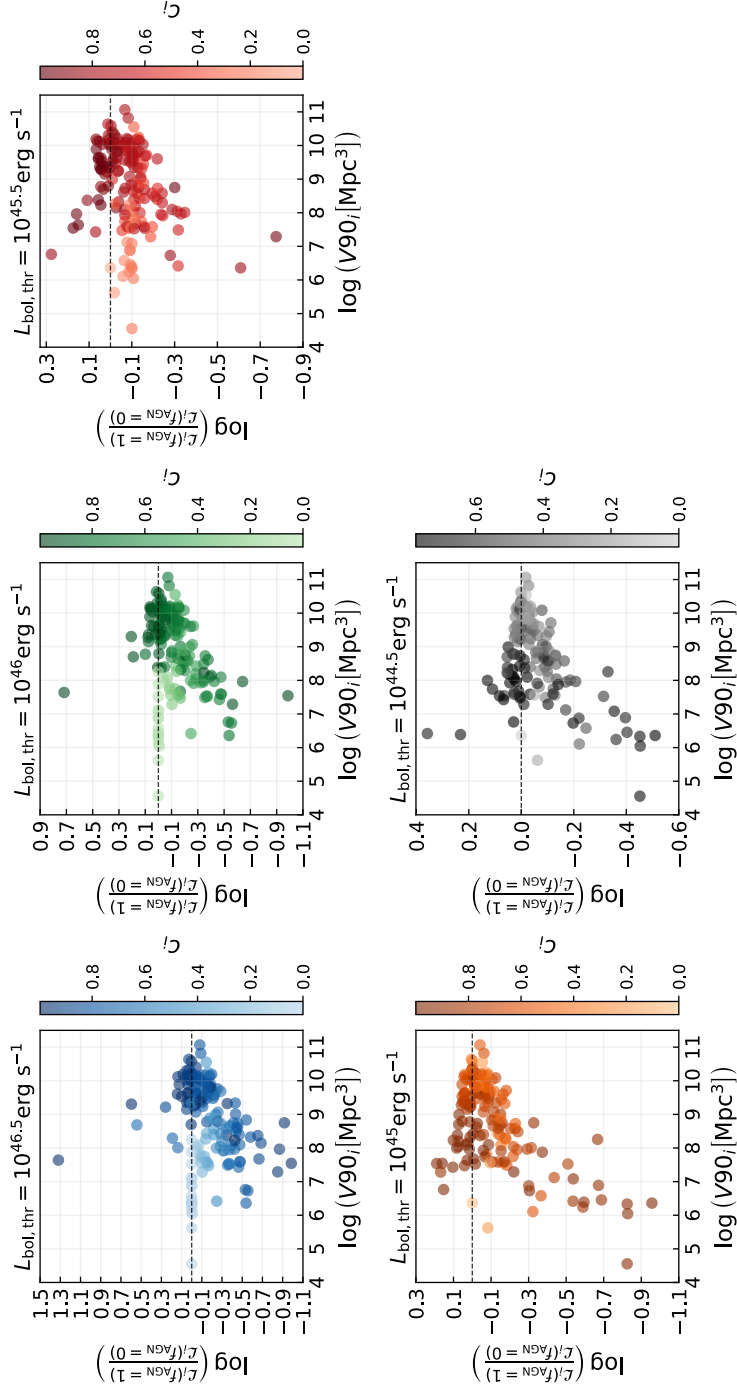
Figure 5.6: Logarithm of the ratio between the value of the single-event likelihood at $f_{\mathrm{AGN}} = 1$ and the one at $f_{\mathrm{AGN}} = 0$ for each detected merger, as a function of the corresponding V90. Each panel shows the results for a different bolometric luminosity threshold. In each plot, the markers are coloured as a function of the average completeness of the AGN catalogue in the region occupied by the 90 per cent CL localisation volume. The dashed horizontal lines mark where $\mathcal{L}_i \left(f_{\mathrm{AGN}} = 1 \right) = \mathcal{L}_i \left(f_{\mathrm{AGN}} = 0 \right)$.

Rounding to the second decimal digit, the right ascensions of the two quasars are 167.22° and 175.58°, their declinations are $-23.64°$ and $-13.35°$, and their redshift estimates from Quaia are 0.37 and 0.40. The values of the number density of the sub-sample of the AGN catalogue with $L_{bol} \geq 10^{46.5} \mathrm{erg\ s^{-1}}$ in the two different redshift bins that contain the two matching quasar candidates are $\approx 10^{-8.86} \mathrm{Mpc^{-3}}$ and $\approx 10^{-8.15} \mathrm{Mpc^{-3}}$. The total probabilities within the 3D credible regions of the GW sky map containing them are ≈ 0.53 and ≈ 0.77.

The value of the single-event likelihood evaluated at $f_{AGN} = 1$ is much higher than the one evaluated at $f_{AGN} = 0$ because two AGN are found within the 90 per cent CL localisation volume while due to random chance 0.06 (0.31) would be expected in the redshift bin with a number density of $n_{AGN} \approx 10^{-8.86} \mathrm{Mpc^{-3}}$ ($n_{AGN} \approx 10^{-8.15} \mathrm{Mpc^{-3}}$), considering the V90 of the GW detection.

While the single-event likelihood function for S240511i favours the hypothesis of an AGN origin, the statistical framework used in this work is focused on analysing the entire population of GW events. The results concerning this specific event are to be considered as hints, not as statistically significant conclusions. Follow-up analyses, conducted especially when the full catalogue of mergers detected during O4 will we published, will be necessary to confidently assess whether or not this merger has an AGN origin.

5.5 Discussion and conclusion

In this work we present new observational constraints on the fractional contribution of the AGN channel to the total observed merger rate of binaries of compact objects, f_{AGN}. These constraints are obtained using the same spatial-correlation-based approach used in Veronesi et al. (2023). With respect to our previous work, we make use of a new, larger dataset, which consists of 159 GW events detected by the interferometers of the LVK collaboration not later than June 1st, 2024, and of the all-sky AGN catalogue Quaia. In particular we use all the AGN contained in this catalogue that have a redshift estimate $z \leq 1.5$ and an absolute value of the galactic latitude $|b| \geq 10°$.

We estimate the bolometric luminosity of every AGN using the magnitudes in the Gaia G_{RP} band. We also estimate the completeness of our catalogue as a function of redshift for different values of bolometric luminosity threshold. The average value of the completeness within the 90 per cent CL localisation volume of each GW event is used during the likelihood maximisation process.

We calculate the posterior probability function on f_{AGN} for different thresholds on the bolometric luminosity. We find that this function always peaks at

$f_{AGN} = 0$. We calculate the upper limits of the 68, 90, and 95 per cent credibility intervals on f_{AGN}. The main results of this work are summarised in Figure 5.5 and in Table 5.3. In particular we estimate that no more than the 21 per cent of the detected GW events used in our analysis originated from an un-obscured AGN with a bolometric luminosity higher than $10^{44.5}$erg s^{-1} with 95 per cent credibility. Objects brighter than such threshold consist of almost the entirety of our Quaia sample. Fainter objects are not included due to the flux limitations of Gaia. Tighter constraints are obtained when higher luminosity thresholds are considered. In particular we find that f_{AGN} is not greater than 11 per cent at a CL of 95 per cent when un-obscured quasars brighter than 10^{45}erg s^{-1} are considered.

Thanks to the increase of a factor ≈ 5 with respect to Veronesi et al. (2023) in the number of used GW events, and to the high level of completeness of the quasar catalogue, we are able to put much tighter constraints on the efficiency of the AGN channel (see Figure 5.5 for a comparison with our previous work).

Our results have been obtained under some assumptions, which are inevitable when inferring the properties of AGN in large catalogues. In order to calculate the bolometric luminosities of the objects of Quaia we have to assume a shape of the typical SED and a value for the bolometric correction. We take the values of these AGN properties from Richards et al. (2006) in order to be consistent with the dataset presented in Wu & Shen (2022), which we use to adjust the bolometric luminosities obtained from Gaia magnitudes. Different assumptions on the SED and on the bolometric correction might lead to different estimates of the bolometric luminosities.

To calculate the completeness of our catalogue, we compare the observed number of AGN with the expected one, which is obtained from the integration of a luminosity function. We choose to use the one presented in Kulkarni et al. (2019) because our bolometric luminosities are calibrated on their SDSS-based estimates from Wu & Shen (2022), and in the redshift range we consider that luminosity function has been fitted on AGN from SDSS, which is a survey that contains un-obscured AGN detectable in the optical band, just like the ones contained in Quaia.

An accurate estimation of the uncertainty on the completeness of the AGN catalogue for each redshift bin and luminosity threshold is non-trivial. Factors that would have to be taken into account are the uncertainty on the measurements of the magnitude in the Gaia G_{RP} band, the potential contamination of the catalogue with stars or galaxies, the uncertainties on the redshift estimates, on the SED shape, and on the bolometric correction. Moreover, the luminosity function we compare the observed number of AGN with has an intrinsic scatter.

With the only exclusion of the first redshift bin of the two sub-samples charac-
terised by the highest luminosity thresholds, the numbers of observed objects
used for the calculation of the completeness (see Figure 5.3) are high enough
for the systematics mentioned above to be considered the dominant source of
uncertainty, since we are in general not limited by low number counts.

As far as our analysis is concerned, taking into consideration the uncertainty
on the completeness is not expected to change the results significantly. This is
because, as described in Section 5.3, we use the average value of the completeness
within the localisation volumes of the GW events to weight the contribution of
each of them to the total likelihood; the constraining power of our method
scales linearly with the completeness of the AGN catalogue, and changes in this
parameter are not expected to lead to any significant variation on the value of
the best estimate for f_{AGN}. For this reason, we choose to use the values of
completeness listed in Table 5.2 throughout our analysis.

Another important caveat to mention is that our analysis and the constraints
we are able to put concern un-obscured AGN, which are visible both in the
optical and in the infrared band. In order to extend our conclusions to the
entire population of AGN, one should take into account what fraction of them
is not visible in the wavelengths observed by Gaia and by WISE, which are the
two surveys from which Quaia has been created from. This obscuration fraction
is in general expected to increase as a function of redshift and to decrease as a
function of luminosity (Merloni et al. 2014; Ueda et al. 2014).

The observational constraints presented in this work consist of a generalisa-
tion of the ones obtained in Veronesi et al. (2023). Here we investigate a wider
range of AGN luminosities and the entirety of the redshift range reached by the
interferometers of the LVK collaboration. For this reason, in order to obtain
in the future even more general results one will need an all-sky AGN catalogue
with a lower threshold in flux with respect to Quaia, to be able to extend the
analysis to the faint-end of the un-obscured AGN population. We estimate that
no more than one GW event out of five has originated in an un-obscured AGN
with a bolometric luminosity higher than $10^{44.5}\mathrm{erg\ s^{-1}}$, but a larger fraction
might still come from fainter objects, or from obscured ones.

While the results of this work demonstrate that the efficiency of the AGN
channel can already be investigated with spatial-correlation analyses using the
currently available data, in the next years it will be possible to put even tighter
constraints using all the events that will be detected in the rest of O4 as well
as the ones that will be detected during the fifth observing run of the LVK
collaboration, O5. Using more data could either reduce the upper limits on
f_{AGN}, or it could cause a shifting of the value of such parameter that maximised

the posterior distribution, moving it away from zero.

Future developments of the statistical method used in this work involve also the introduction of physically-motivate priors on the intrinsic binary properties. Different binary formation channels are indeed expected to produce different features in the distributions of the masses and the spins of the merging systems, as well as on their eccentricity. The analysis here presented has been kept purposely agnostic as far as the physics of the formation mechanism is concerned. Introducing physically-motivated changes in the likelihood function might result in different constraints on f_{AGN} and will inform us on which are the intrinsic binary parameters that are able to add more information to the analysis.

Acknowledgements

Data Availabilty

The AGN catalogue used in this work, the results of the cross-matches, and related data products are publicly available at https://zenodo.org/records/12805938. The code used to produce the results presented in this paper will be shared on reasonable request to the corresponding author.